Subperiodic trigonometric subsampling: a numerical approach *

Alvise Sommariva and Marco Vianello†
Department of Mathematics, University of Padova (Italy)

February 17, 2017

Abstract

We show that Gauss-Legendre quadrature applied to trigonometric polynomials on subintervals of the period can be competitive with subperiodic trigonometric Gaussian quadrature. For example with intervals corresponding to few angular degrees, relevant for regional scale models on the earth surface, we see a subsampling ratio of one order of magnitude already at moderate trigonometric degrees.

2010 AMS subject classification: 65D32, 65T40.

Keywords: subperiodic trigonometric quadrature, subsampling, numerical cubature on regions of the sphere.

1 Subsampling for trigonometric quadrature

In recent years some attention has been devoted in the numerical literature to trigonometric approximation on subintervals of the period. Relevant topics are the theory of Fourier extensions, where one of the main initial motivations was of circumventing the Gibbs phenomenon (cf., e.g., [1, 2, 7]), and the theory of subperiodic interpolation and quadrature, whose main motivation came from polynomial approximation on domains related to circular/elliptical arcs, such as sections of disk and sphere (cf., e.g., [6, 8, 10, 16]).

In this note, which is essentially of computational character, we focus on the quadrature setting. For the reader's convenience, we report the main result of [10] concerning *subperiodic trigonometric Gaussian quadrature*. Below, we shall denote by $\mathbb{T}_n$ the $(2n+1)$-dimensional space of univariate trigonometric polynomials of degree not exceeding n.

Setting $\alpha = \sin(\omega/2)$, by the nonlinear transformation $\theta = 2\arcsin(\alpha x)$, $x \in [-1,1]$, we can write for any integrable f

$$\int_{-\omega}^{\omega} f(\theta)\,d\theta = \int_{-1}^{1} f(2\arcsin(\alpha x))\,w(x)\,dx\ , \quad w(x) = \frac{2\alpha}{\sqrt{1-\alpha^2\,x^2}}\ . \tag{1}$$

*Work partially supported by the DOR funds and by the biennial projects CPDA124755 and BIRD163015 of the University of Padova, and by the GNCS-INdAM.

†Corresponding author: e-mail: *marcov@math.unipd.it*

Then, we have the following result (cf. [10])

Theorem 1 *Let be* $0 < \omega \leq \pi$ *and let* $\{(x_j, \lambda_j)\}_{1 \leq j \leq n+1}$ *be the nodes and positive weights of the algebraic Gaussian quadrature formula for the weight function* $w(x)$ *in (1).*

Then

$$\int_{-\omega}^{\omega} t(\theta)\, d\theta = \sum_{j=1}^{n+1} \lambda_j t(\theta_j)\ , \quad \forall t \in \mathbb{T}_n\ , \tag{2}$$

where $\theta_j = 2 \arcsin(\alpha\, x_j) \in (-\omega, \omega)$, $j = 1, 2, \ldots, n+1$.

Concerning algebraic Gaussian quadrature see, e.g., [13], [19, Ch. 5]. Observe that, since the weight function $w(x)$ in (1) is even, the set of angular nodes is symmetric, and that symmetric nodes have equal weight, cf. [13, Ch. 1].

Formula (2) has been termed Gaussian since it is exact on a space of dimension $2n+1$ with $n+1$ nodes. Unlike algebraic Gaussian formulas the nodes and weights cannot be tabulated in a reference subinterval, and have to be recomputed when ω changes. In [9, 10] a Chebyshev moment-based algorithm has been used; an alternative method could resort to the more general sub-range Jacobi polynomials approach, studied in [15].

On the other hand, we can also simply write, for any integrable f,

$$\int_{-\omega}^{\omega} f(\theta)\, d\theta = \omega \int_{-1}^{1} f(\omega x)\, dx\ , \tag{3}$$

and think to apply the standard Gauss-Legendre formula to this integral. Of course, we do not expect trigonometric exactness now, but which could be the number of nodes that guarantees an error not far from machine precision, for the trigonometric basis $\{1, \cos(k\theta), \sin(k\theta), 1 \leq k \leq n\}$? Perhaps not surprisingly, this number, can be much lower than $n+1$ for "small" ω.

Indeed, we have chosen the number of nodes, say $\nu_\varepsilon(n, \omega)$, as the smallest integer ν such that, denoting by $\{(\xi_j, w_j)\}$, $1 \leq j \leq \nu$, the nodes and weights of the Gauss-Legendre formula, we get

$$\begin{aligned}
&\left| \int_{-1}^{1} \cos(k\omega x)\, dx - \sum_{j=1}^{\nu} w_j\ \cos(k\omega\xi_j) \right| = \left| \frac{2\sin(k\omega)}{k\omega} - \sum_{j=1}^{\nu} w_j\ \cos(k\omega\xi_j) \right| < \varepsilon\ , \\
&\left| \int_{-1}^{1} \sin(k\omega x)\, dx - \sum_{j=1}^{\nu} w_j\ \sin(k\omega\xi_j) \right| = \left| \sum_{j=1}^{\nu} w_j\ \sin(k\omega\xi_j) \right| < \varepsilon\ , \quad 1 \leq k \leq n\ ,
\end{aligned} \tag{4}$$

with $\varepsilon = 10^{-14}$ ($\sin(k\omega x)$ being an odd function). See Figure 2-right and Figure 3, where the essential behavior of the ratio $(n+1)/\nu_\varepsilon(n, \omega)$ is displayed (the quantity $\tilde{g}_\varepsilon(n\omega)$ is very close to $\nu_\varepsilon(n, \omega)$).

We can give a qualitative explanation of such a behavior observing that the functions $\cos(k\omega x), \sin(k\omega x)$ are well-approximated by polynomials of degree not much larger than $k\omega$ on $[-1, 1]$. In fact, considering the Chebyshev expansions [18, §3.3.2]

$$\cos(k\omega x) = \sum_{j=0}^{\infty} c_j (-1)^j J_{2j}(k\omega) T_{2j}(x)\ , \quad c_0 = 1\ ,\ c_j = 2\ ,\ j > 0\ ,$$

$$\sin(k\omega x) = \sum_{j=0}^{\infty} (-1)^j J_{2j+1}(k\omega) T_{2j+1}(x) \ , \quad x \in [-1,1] \ , \tag{5}$$

together with a classical estimate for Bessel functions of the first kind [20, §2.9] and Stirling's formula

$$|J_s(k\omega)| \leq \frac{(k\omega/2)^s}{s!} \sim \left(\frac{ek\omega}{2s}\right)^s \frac{1}{\sqrt{2\pi s}} \ , \quad s \to \infty \ , \tag{6}$$

we have that the Chebyshev cofficients decay very rapidly for $2j > ek\omega/2$.

Now, we need to connect theoretically the "moment errors" in (4) with the integration error for a generic function. This connection is given by the following result, that was essentially proved in [22] in the multivariate polynomial setting and we report here for convenience in a general univariate framework.

Theorem 2 *Let $\mathcal{S} = \langle \phi_1, \ldots, \phi_N \rangle$ be an N-dimensional space of continuous univariate functions in $[a,b]$, where the basis $\{\phi_i\}$ is orthonormal with respect to a measure λ on $[a,b]$. Let μ be a measure on $[c,d] \subseteq [a,b]$ and $\{(t_j, \sigma_j)\}$, $1 \leq j \leq M$, the nodes and positive weights of a quadrature formula for μ, exact on constant functions; define*

$$\varepsilon_i = \int_c^d \phi_i(t)\, d\mu - \sum_{j=1}^{M} \sigma_j\, \phi_i(t_j) \ , \quad 1 \leq i \leq M \ , \quad \varepsilon_{mom} = \|\{\varepsilon_i\}\|_2 \ . \tag{7}$$

Then, for every $f \in C[a,b]$ the following quadrature error estimate holds

$$\left| \int_c^d f(t)\, d\mu - \sum_{j=1}^{M} \sigma_j\, f(t_j) \right| \leq C \min_{\phi \in \mathcal{S}} \|f - \phi\|_{\infty,[a,b]} + \|f\|_{L^2_\lambda(a,b)}\, \varepsilon_{mom} \ , \tag{8}$$

where

$$C = 2\mu([c,d]) + \sqrt{\lambda([a,b])}\, \varepsilon_{mom} \ .$$

Proof. First, observe that

$$\int_c^d \phi(t)\, d\mu = \langle \boldsymbol{\gamma}, \boldsymbol{m} \rangle \ , \quad \forall \phi \in \mathcal{S} \ , \tag{9}$$

$\boldsymbol{\gamma} = \{\gamma_i\}$, $\boldsymbol{m} = \{m_i\}$, $1 \leq i \leq M$, where

$$\gamma_i = \frac{\int_a^b \phi(t)\phi_i(t)\, d\lambda}{\left(\int_a^b \phi_i^2(t)\, d\lambda\right)^{1/2}} \ , \quad m_i = \int_c^d \phi_i(t)\, d\mu \ ,$$

are the Fourier coefficients of ϕ in the λ-orthogonal basis $\{\phi_i\}$ and the μ-moments of $\{\phi_i\}$ on $[c,d]$, respectively. Moreover,

$$\sum_{j=1}^{M} \sigma_j\, \phi(t_j) = \langle \boldsymbol{\gamma}, \widetilde{\boldsymbol{m}} \rangle \ , \quad \widetilde{m}_i = \sum_{j=1}^{M} \sigma_j\, \phi_i(t_j) \ , \tag{10}$$

where $\widetilde{\boldsymbol{m}}$ are the approximate moments, the 2-norm of the moment error being denoted by ε_{mom} in (7).

Then we can write the "*near exactness*" estimate

$$\left| \int_c^d \phi(t)\, d\mu - \sum_{j=1}^{M} \sigma_j\, \phi(t_j) \right| = |\langle \boldsymbol{\gamma}, \boldsymbol{m} - \widetilde{\boldsymbol{m}} \rangle|$$

$$\leq \|\boldsymbol{\gamma}\|_2\, \|\boldsymbol{m} - \widetilde{\boldsymbol{m}}\|_2 = \|\phi\|_{L^2_\lambda(a,b)}\, \varepsilon_{mom}\ . \tag{11}$$

Now, take $f \in C([a,b])$, and let ϕ^* be an element of minimum distance of $\mathcal{S}$ from f in the uniform norm on $[a,b]$, i.e. $\|f-\phi^*\|_{\infty,[a,b]} = \min_{\phi\in\mathcal{S}} \|f-\phi\|_{\infty,[a,b]}$. By a classical chain of inequalities in quadrature theory and (11) we get

$$\left| \int_c^d f(t)\, d\mu - \sum_{j=1}^{M} \sigma_j\, f(t_j) \right| \leq \left| \int_c^d f(t)\, d\mu - \int_c^d \phi^*(t)\, d\mu \right|$$

$$+ \left| \int_c^d \phi^*(t)\, d\mu - \sum_{j=1}^{M} \sigma_j\, \phi^*(t_j) \right| + \left| \sum_{j=1}^{M} \sigma_j\, \phi^*(t_j) - \sum_{j=1}^{M} \sigma_j\, f(t_j) \right|$$

$$\leq \left(\mu([c,d]) + \sum_{j=1}^{M} \sigma_j \right) \min_{\phi\in\mathcal{S}} \|f-\phi\|_{\infty,[a,b]} + \|\phi^*\|_{L^2_\lambda(a,b)}\, \varepsilon_{mom}\ .$$

By exactness of the quadrature formula on constant functions and the inequality

$$\|\phi^*\|_{L^2_\lambda(a,b)} \leq \|\phi^*-f\|_{L^2_\lambda(a,b)} + \|f\|_{L^2_\lambda(a,b)} \leq \sqrt{\lambda([a,b])}\, \|f-\phi^*\|_{\infty,[a,b]} + \|f\|_{L^2_\lambda(a,b)}\ ,$$

we finally obtain (8). □

In the present trigonometric framework Theorem 2 can be applied with $\mathcal{S} = \mathbb{T}_n$ and $N = \dim(\mathbb{T}_n) = 2n+1$, $[a,b] = [-\pi,\pi]$, $[c,d] = [-\omega,\omega]$, $d\mu = d\lambda = d\theta$; the quadrature formula is the scaled Gauss-Legendre formula $\{(t_j,\sigma_j)\} = \{(\omega\xi_j, \omega w_j)\}$ and $M = \nu_\varepsilon(n,\omega)$, cf. (3)-(4). In particular, the moment error can be bounded as

$$\varepsilon_{mom} \leq \varepsilon\, \omega \sqrt{2n+1}\ . \tag{12}$$

2 Implementation and examples

The key observation for an effective implementation of Gauss-Legendre quadrature in the subperiodic trigonometric setting is the following. Consider the trigonometric functions $\cos(ux)$, $\sin(ux)$, $x \in [-1,1]$, where u is a positive parameter (we are clearly interested in $u = n\omega$). Define as $g_\varepsilon(u)$ the minimum number of Gauss-Legendre nodes such that

$$\mathcal{E}(u) = \max \left\{ \left| \frac{2\sin(u)}{u} - \sum_{j=1}^{g_\varepsilon(u)} w_j\, \cos(u\xi_j) \right|, \left| \sum_{j=1}^{g_\varepsilon(u)} w_j\, \sin(u\xi_j) \right| \right\} < \varepsilon \tag{13}$$

for a fixed $\varepsilon > 0$. It turns out, at least numerically, that g_ε is a *nondecreasing* function of $u > 0$. Then, we have that the integer function ν_ε in (4) is simply

$$\nu_\varepsilon(n, \omega) = g_\varepsilon(n\omega) \; . \tag{14}$$

Though we have not a rigorous proof but only numerical evidence of the monotonicity of g (see e.g. Figure 1), this property appears quite natural. Indeed, taking for example $\cos(ux)$, consider the classical Gauss-Legendre quadrature error estimate with $s+1$ nodes, namely $4E_{2s+1}(\cos(u\,\cdot); [-1, 1])$, where $E_m(f; [a, b]) = \min_{p \in \mathbb{P}_m} \|f - p\|_{\infty,[a,b]}$ is the best uniform approximation error by polynomials of degree m for $f \in C[a, b]$. Now, such an estimate is a nondecreasing function of u, since, as it can be easily proved, $E_m(\cos(u\,\cdot); [-1, 1]) = E_m(\cos(\cdot); [-u, u])$. The same holds for $\sin(ux)$, and hence computing $g_\varepsilon(u)$ from the Gauss-Legendre error estimates would give a number of Gauss-Legendre nodes nondecreasing in u.

In practice, the direct computation of $g_\varepsilon(u)$ by applying iteratively the Gauss-Legendre formula is costly (especially at high frequencies), while resorting to the Gauss-Legendre quadrature error estimates gives typically a substantial overestimate of the number of nodes. Thus, we have chosen an alternative numerical approach.

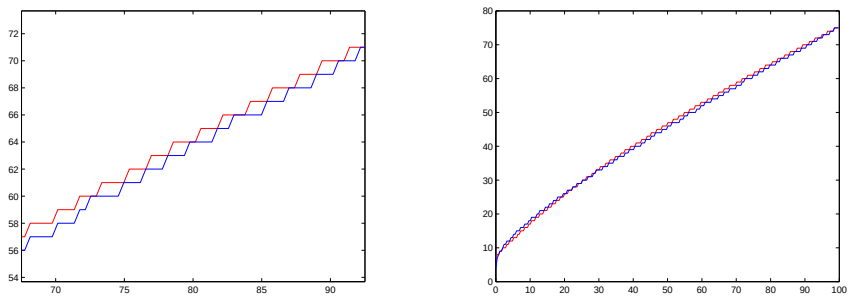

Figure 1: The integer valued functions $g_\varepsilon(u)$ (blue) and $\tilde{g}_\varepsilon(u)$ (red) in the interval $[\pi/180, 100]$ (right: detail).

First, we have chosen $\varepsilon = 10^{-14}$, in view of the numerical evidence that, working in double precision, it is difficult to go much below such a threshold with the moment errors in the whole ω range (a fact that has been observed also in [10] concerning subperiodic trigonometric Gaussian quadrature). Then, once and for all, we have sampled $g_\varepsilon(u)$ at a relatively small number of nodes in the interval $[1, 500]$ and constructed the cubic spline interpolant to such values, say $s_3(u)$ (observe that $u = n\omega = 500$ corresponds to n in the hundreds even for $\omega = \pi$). In practice, we have sampled at 21 equispaced nodes in $[1, 500]$ and the corresponding 21 values of g_ε are the only information to be stored. Then we have taken

$$\tilde{g}_\varepsilon(u) = \lceil s_3(u) \rceil \; , \quad u \in (0, 500] \; , \tag{15}$$

observing an average discrepancy $|g_\varepsilon(u) - \tilde{g}_\varepsilon(u)|$ of about 0.7 on a fine control mesh in $[\pi/180, 500]$ (the values being extrapolated by the first cubic for $u < 1$).

The corresponding quadrature errors are displayed in Figure 2-left, where we see that using $\tilde{g}_\varepsilon(u)$ instead of $g_\varepsilon(u)$ they remain below $0.5\,10^{-13}$. No substantial

improvement in the performance has been observed by increasing the number of sampled values or taking the left-hand side of the interval smaller than 1. For higher frequencies, the number $g_\varepsilon(u)$ is well-approximated by linear regression, and we have seen a good behavior of quadrature taking

$$\tilde{g}_\varepsilon(u) = 0.54u + 21\ , \quad u > 500\ . \tag{16}$$

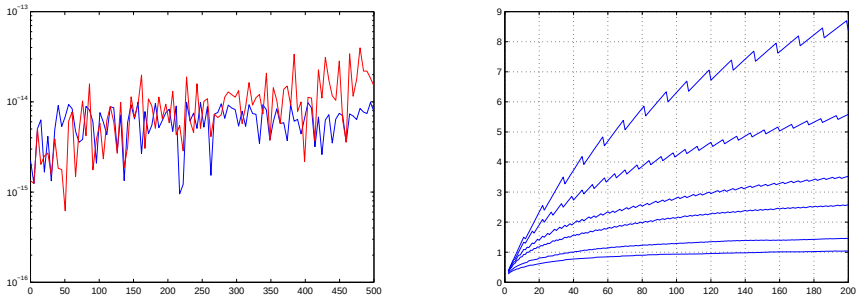

Figure 2: Left: the error $\mathcal{E}(u)$ in (13) (log scale) computed with $g_\varepsilon(u)$ (blue) and $\tilde{g}_\varepsilon(u)$ for $u \in [\pi/180, 500]$. Right: the ratio $(n+1)/\tilde{g}_\varepsilon(n\omega)$ up to trigonometric degree 200 at (from top to bottom) $\omega = \pi/36, \pi/18, \pi/9, \pi/6, \pi/3, \pi/2$ (corresponding to an angular interval of 10, 20, 40, 60, 120, 180 degrees).

In Figure 2-right we have displayed the ratio

$$\rho_n(\omega) = \frac{n+1}{\tilde{g}_\varepsilon(n,\omega)} \tag{17}$$

for $n = 1, \ldots, 200$ at different values of ω, where can see a remarkable subsampling effect correspondingly to the smaller angular intervals. For example, at $\omega = \pi/36$, corresponing to an angular interval of 10 degrees, we can subsample by a factor 5 already for trigonometric degree $n = 60$. A contour plot of the same ratio as a bivariate function of (ω, n) is shown in Figure 3.

Observe that from the empirical formula (16) we expect in practice a subsampling effect (at least for large k) only for $0.54\,\omega < 1$, that is $\omega < 1.85$ or equivalently $\omega < 0.59\,\pi$ (which is in good accordance with the observed behavior). On the other hand, the asymptotic analysis in (5)-(6) would suggest a little more restrictive range, namely $\omega < 4/e \approx 1.47$ or equivalently $\omega < 0.46\,\pi$.

In order to make some meaningful examples, we have modified the Matlab function `trigauss` in the software package [9], in such a way that Gauss-Legendre quadrature is chosen as soon as $\tilde{g}_\varepsilon(n\omega) < n+1$. When a generic angular interval $[\alpha, \beta]$, with $\beta - \alpha \leq 2\pi$, is concerned, the variable is simply shifted as $\theta' = \theta - (\alpha+\beta)/2$, with $\theta' \in [-\omega, \omega]$, $\omega = (\beta - \alpha)/2$.

2.1 Circular sections

We start from the following simple observation: a multivariate polynomial of total degree n restricted to an arc of a circle is a univariate trigonometric polynomial of degree n. This fact has allowed to construct algebraic cubature formulas

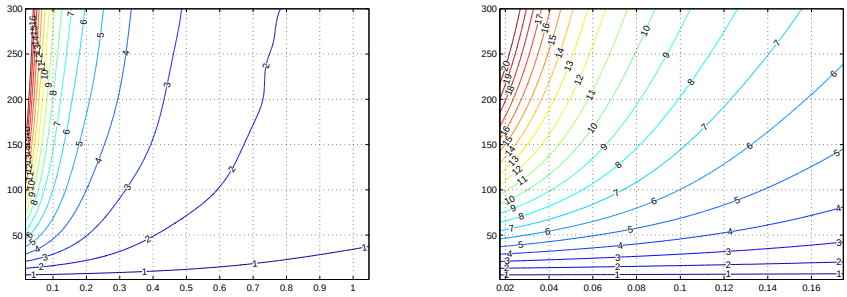

Figure 3: Contour plot of the ratio $(n+1)/\tilde{g}_\varepsilon(n\omega)$ for $n = 1, \ldots, 300$, $\omega \in [\pi/180, \pi/3]$ (left) and detail for $\omega \in [\pi/180, \pi/18]$ (right).

on several multivariate domains related to circular arcs, cf. e.g. [8, 10, 12, 16]. Applications arise, for example, in the field of optical design [3].

Several instances of disk sections, such as circular segments, sectors, zones, lenses, can be treated in the general framework of linear blending of arcs. We do not go into details here, addressing the interested reader to [8], but we only recall that all such cases fall into the class of domains

$$\Omega = \tau([0,1] \times [\alpha, \beta]) \ , \quad \beta - \alpha \leq 2\pi \ ,$$

$$\tau(t,\theta) = (\tau_1(t,\theta), \tau_2(t,\theta)) \ , \quad \tau_i(t,\theta) \in \mathbb{P}_1 \otimes \mathbb{T}_1 \ , \ i = 1,2 \ , \tag{18}$$

where the blending transformation τ has constant sign Jacobian $|\det(J\tau)| = \pm\det(J\tau) \in \mathbb{P}_1 \otimes \mathbb{T}_2$, and thus

$$\int_\Omega f(x,y)\, dxdy = \int_0^1 \int_\alpha^\beta f(\tau(t,\theta))\, |\det(J\tau(t,\theta))|\, d\theta dt \ . \tag{19}$$

Now, if $f \in \mathbb{P}_n^2$, then $(f \circ \tau)\, |\det(J\tau)| \in \mathbb{P}_{n+1} \otimes \mathbb{T}_{n+2}$, and we can construct a cubature formula with polynomial exactness, simply as a product formula of Gauss-Legendre quadrature in the radial direction with exact trigonometric Gaussian quadrature in the angular direction. On the other hand, we can substitute the exact trigonometric Gaussian quadrature with the nearly-exact Gauss-Legendre formula in (13). In special cases, $|\det(J\tau)|$ can be independent of one of the variables, as with circular sectors, $|\det(J\tau)| = Rt$, or circular segments, $|\det(J\tau)| = R^2 \sin^2(\theta)$ (R being the circle radius), cf. [8, 10].

As an example, we have taken two circular sectors of the unit disk

$$\tau = (t\cos(\theta), t\sin(\theta)) \ , \quad t \in [0,1] \ , \quad \theta \in [-\omega, \omega] \ ,$$

corresponding to angles $2\omega = \pi/3$ (60 angular degrees) and $2\omega = \pi/18$ (10 angular degrees). Here, the subsampling ratio at the same degree of exactness n is $\rho_n(\omega)$ in (17). Near exactness in the cubature of polynomials of the form $(ax+by+2)^n$, where a and b are uniform random variables in $[-1,1]$, is shown in Figure 4-top (averages of 100 random samples), whereas the subsampling ratios are displayed in Figure 4-bottom.

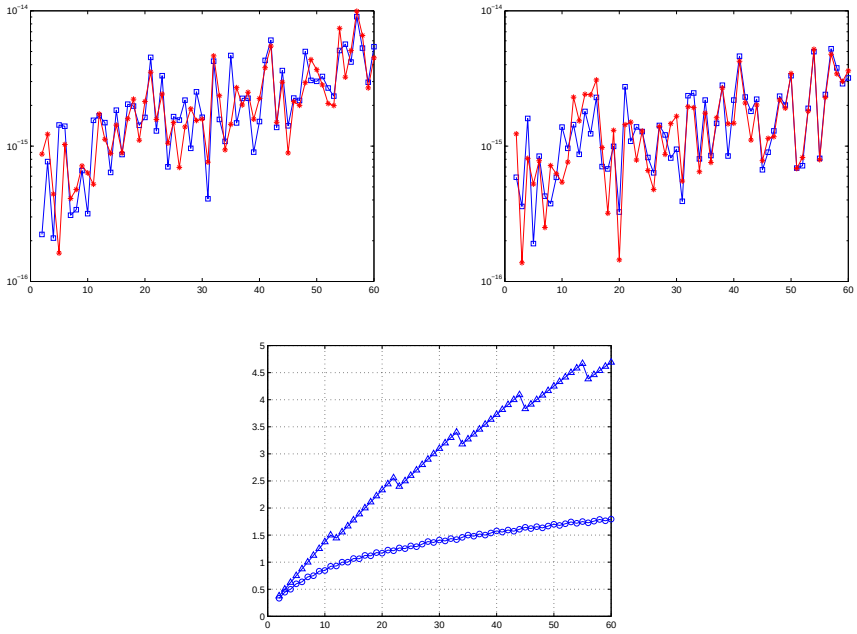

Figure 4: Top: relative cubature error for random polynomials of degree $2, \cdots, 60$ on a circular sector with angle of 60 degrees (left) and 10 degrees (right), by exact trigonometric Gaussian quadrature (blue squares) and nearly-exact Gauss-Legendre subsampling (red stars). Bottom: subsampling ratio for the 60 degree arc (circles) and the 10 degree arc (triangles).

2.2 Spherical sections

We present now examples concerning numerical cubature on special sections of the unit sphere S^2, a subject that has received some attention in the recent literature, cf. e.g. [4, 5, 16, 17]. Consider the spherical coordinates

$$(x, y, z) = \sigma(\theta, \varphi) = (\cos(\theta)\sin(\varphi), \sin(\theta)\sin(\varphi), \cos(\varphi)) \ , \tag{20}$$

where θ is the azimuthal angle and φ the polar angle, $(\theta, \varphi) \in [-\pi, \pi] \times [0, \pi]$, and a "geographic rectangle", that is

$$\Omega = \sigma([\alpha_1, \beta_1] \times [\alpha_2, \beta_2]) \ , \quad [\alpha_1, \beta_1] \subseteq [-\pi, \pi] \ , \quad [\alpha_2, \beta_2] \subseteq [0, \pi] \ . \tag{21}$$

To compute the corresponding surface integral we can write

$$\begin{aligned} \int_\Omega f(x, y, z)\, dS &= \int_{\alpha_1}^{\beta_1} \int_{\alpha_2}^{\beta_2} f(\sigma(\theta, \varphi)\, |\sin(\varphi)|\, d\varphi\, d\theta \ , \\ &= \int_{\alpha_1}^{\beta_1} \int_{\alpha_2}^{\beta_2} f(\sigma(\theta, \varphi)\ \sin(\varphi)\, d\varphi\, d\theta \ . \end{aligned} \tag{22}$$

Observing that if $f \in \mathbb{P}_n^3(S^2)$, then $(f \circ \sigma)\ \sin(\varphi) \in \mathbb{T}_n \otimes \mathbb{T}_{n+1}$, we can construct a cubature formula with polynomial exactness and cardinality $(n+1)(n+2)$,

simply as a product formula of exact trigonometric Gaussian quadrature in the two angles.

Notice that spherical caps are special cases of geographic rectangles, where the azimuthal angle corresponds to a complete circle. Consider indeed (up to rotations) a *polar cap* with an arc of length 2ω, that is described in spherical coordinates as

$$\Omega = \sigma([-\pi, \pi] \times [0, \omega]) \, . \tag{23}$$

Here symmetry can be used to reduce the number of nodes of the original formulas to $n^2/2 + \mathcal{O}(n)$ (cf. [16, 17]).

Now, we can substitute the exact trigonometric Gaussian quadrature with the nearly-exact Gauss-Legendre formula in (13); in this case, a "product effect" in the subsampling arises, at least for $\omega_1, \omega_2 < 0.59\,\pi$ (see the empirical considerations after (17)). Indeed, the subsampling ratio at the same degree of exactness n becomes $\rho_n(\omega_1)\,\rho_{n+1}(\omega_2)$, cf. (17), where $\omega_1 = (\beta_1 - \alpha_1)/2$ and $\omega_2 = (\beta_2 - \alpha_2)/2$, since both the variables are involved. In the case of a spherical (polar) cap (23), subsampling acts only on the polar angle.

We make some examples concerning geographic rectangles of the earth surface, from a continental to a regional scale (notice that a scaling of the Cartesian variables by the earth radius is implicit). In the first example we have considered two spherical (polar) caps, one corresponding to latitudes over $60^o N$ (arc of 60 degrees, $\omega = \pi/6$) and the second to latitudes over $85^o N$ (arc of 10 degrees, $\omega = \pi/36$).

The results are collected in Figure 5. Near exactness in the cubature of polynomials of the form $(ax + by + cz + 3)^n$, where a, b, c are uniform random variables in $[-1, 1]$, is shown in Figure 5-top (averages of 100 random samples). We recall that the cardinality of the formulas in [17] is approximately $(n+1)(n+2)/2$ whereas that of the formula in [16] is approximately $(n+1)^2/2$, both leading to a subsampling ratio with respect to the present formula (whose cardinality is $(n+1)\tilde{g}_\varepsilon((n+1)\omega/2)$ since the φ-interval half-length is $\omega/2$) of approximately $\frac{1}{2}\rho_{n+1}(\omega/2)$; see Figure 5-bottom. To have an idea, on the smaller cap for polynomial degree 30 we use 279 versus the 496 nodes of [17], and for degree 60 we use 610 versus 1891 nodes.

For the second example, we have taken two geographic rectangles. The first

$$\Omega_1 = \sigma\left(\left[-\frac{125}{180}\,\pi, -\frac{67}{180}\,\pi\right] \times \left[\frac{41}{180}\,\pi, \frac{65}{180}\,\pi\right]\right) \, , \quad \omega_{11} \approx 0.506 \, , \quad \omega_{12} \approx 0.209 \, , \tag{24}$$

corresponds in standard longitude-latitude to $67^o W$ - $125^o W$, $25^o N$ - $49^o N$, a vaste rectangle approximately containing the contiguous continental USA, whereas the second

$$\Omega_2 = \sigma\left(\left[-\frac{109}{180}\,\pi, -\frac{102}{180}\,\pi\right] \times \left[\frac{49}{180}\,\pi, \frac{53}{180}\,\pi\right]\right) \, , \quad \omega_{21} \approx 0.061 \, , \quad \omega_{22} \approx 0.035 \, , \tag{25}$$

is the rectangle $102^o W$ - $109^o W$, $37^o N$ - $41^o N$, corresponding to Colorado.

The results are collected in Figure 6. The random polynomials are as in the cap example. The product effect is clearly visible in Figure 6-bottom, and is stronger for the smaller rectangle (Colorado). To have an idea, on the Colorado rectangle for polynomial degree 30 we use 81 versus the 992 nodes of [16], and

for degree 60 we use 110 versus 3782 nodes (the subsampling ratio is of about one order of magnitude already for degree 25).

It is worth stressing that the fact of being on a sphere is not essential, since such results would have been obtained for example also on rectangles of the torus, with angular intervals (in the usual poloidal-toroidal coordinates) of the same length of those in (24)-(25). On the other hand, nearly-exact Gauss-Legendre subsampling can be adopted also for product formulas on solid sections, for example spherical sectors whose base is a cap or more generally a geographic rectangle, keeping the corresponding subsampling ratios.

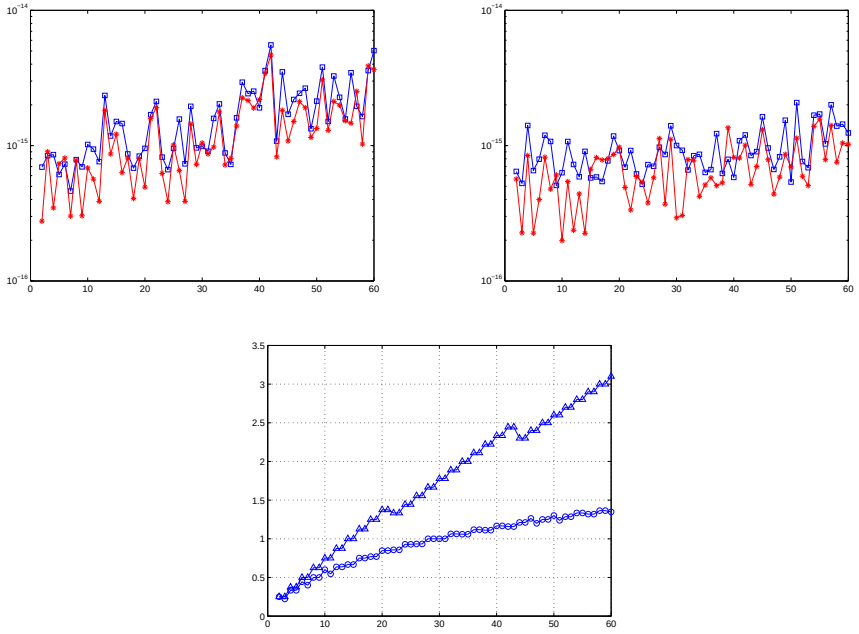

Figure 5: Top: relative cubature error for random polynomials for degree $2, \cdots, 60$ on polar caps with latitude over 60^oN (left) and 85^oN (right), by exact trigonometric Gaussian quadrature (blue squares) and nearly-exact Gauss-Legendre subsampling (red stars). Bottom: subsampling ratio for the 60^oN (circles) and the 85^oN cap (triangles).

2.3 Conclusions and future work

This numerical paper is only a first step towards the comprehension of the subsampling phenomenon in subperiodic trigonometric approximation and quadrature. We have shown that nearly-exact Gauss-Legendre quadrature can be competitive with exact subperiodic trigonometric Gaussian quadrature [10], especially when product formulas are involved. We plan to adopt such nearly-exact quadrature formulas in all our codes for algebraic cubature on multivariate domains constructed via circular arcs, such as sections of disk, sphere, torus [9].

On the other hand, some preliminary tests have revealed that a similar subsampling phenomenon seems to arise directly with subperiodic trigonometric

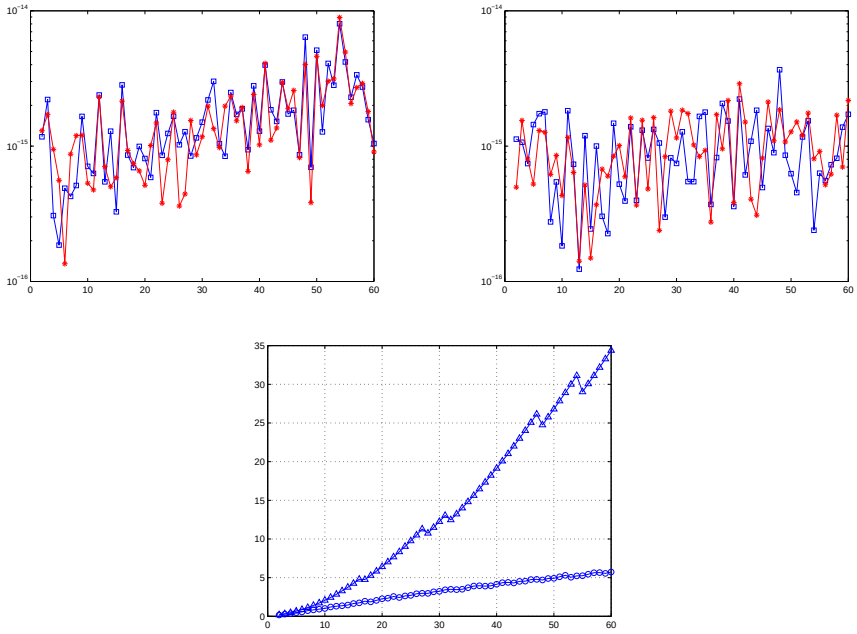

Figure 6: Top: relative cubature error for random polynomials for degree $2, \cdots, 60$ on geographic rectangles corresponding to USA (left) and Colorado (right), by exact trigonometric Gaussian quadrature (blue squares) and nearly-exact Gauss-Legendre subsampling (red stars). Bottom: subsampling ratio for USA (circles) and Colorado (triangles).

Gaussian quadrature, in the sense that nearly-exact quadrature seems to require less nodes than the exact one, depending on the length of the angular interval. Or equivalently, that near-exactness seems to occur up to a higher trigonometric degree than the nominal exactness one.

This phenomenon, as well as a comparison with the popular quadrature methods based on prolate spheroidal wave functions (cf., e.g., [21] and references therein), deserve future investigation.

References

[1] B. Adcock and D. Huybrechs, On the resolution power of Fourier extensions for oscillatory functions, J. Comput. Appl. Math. 260 (2014) 312–336.

[2] B. Adcock, D. Huybrechs and J.M. Vaquero, On the numerical stability of Fourier extensions, Found. Comput. Math. 14 (2014), 635–687.

[3] B. Bauman and H. Xiao, Gaussian quadrature for optical design with non-circular pupils and fields, and broad wavelength range, Proc. SPIE, 7652(2) (2010), 1–12.

[4] J. Beckmann, H.N. Mhaskar and J. Prestin, Quadrature formulas for integration of multivariate trigonometric polynomials on spherical triangle, GEM-International Journal on Geomathematics 3 (2012), 119–138.

[5] J. Beckmann, H.N. Mhaskar and J. Prestin, Local numerical integration on the sphere, GEM-International Journal on Geomathematics 5 (2014), 143–62.

[6] L. Bos and M. Vianello, Subperiodic trigonometric interpolation and quadrature, Appl. Math. Comput. 218 (2012), 10630–10638.

[7] J.P. Boyd, A comparison of numerical algorithms for Fourier extension of the first, second, and third kinds, J. Comput. Phys. 178 (2002), 118–160.

[8] G. Da Fies, A. Sommariva and M. Vianello, Algebraic cubature by linear blending of elliptical arcs, Appl. Numer. Math. 74 (2013), 49–61.

[9] G. Da Fies, A. Sommariva and M. Vianello, SUBP: Matlab package for subperiodic trigonometric quadrature and multivariate applications, online at: `http://www.math.unipd.it/~marcov/CAAsoft.html`.

[10] G. Da Fies and M. Vianello, Trigonometric Gaussian quadrature on subintervals of the period, Electron. Trans. Numer. Anal. 39 (2012), 102–112.

[11] G. Da Fies and M. Vianello, Algebraic cubature on planar lenses and bubbles, Dolomites Res. Notes Approx. 5 (2012), 7–12.

[12] G. Da Fies and M. Vianello, Product Gaussian quadrature on circular lunes, Numer. Math. Theory Methods Appl. 7 (2014), 251–264.

[13] W. Gautschi, Orthogonal Polynomials: Computation and Approximation, Oxford University Press, New York, 2004.

[14] W. Gautschi, Orthogonal polynomials (in Matlab), J. Comput. Appl. Math. 178 (2005), 215–234, software online at:
`http://www.cs.purdue.edu/archives/2002/wxg/codes`.

[15] W. Gautschi, Sub-range Jacobi polynomials, Numer. Algorithms 61 (2012), 649–657.

[16] M. Gentile, A. Sommariva and M. Vianello, Polynomial approximation and quadrature on geographic rectangles, Appl. Math. Comput., published online 25 November 2016.

[17] K. Hesse and R.S. Womersley, Numerical integration with polynomial exactness over a spherical cap, Adv. Comput. Math. 36 (2012), 451–483.

[18] Y.L. Luke, Mathematical Functions and their Approximations, Academic Press, New York-London, 1975.

[19] G. Mastroianni and G.V. Milovanovic, Interpolation processes. Basic theory and applications, Springer Monographs in Mathematics, Springer-Verlag, Berlin, 2008.

[20] F.W.J. Olver, Asymptotics and special functions. Academic Press, New York-London, 1974.

[21] A. Osipov and V. Rokhlin, On the evaluation of prolate spheroidal wave functions and associated quadrature rules, Appl. Comput. Harmon. Anal. 36 (2014), 108–142.

[22] A. Sommariva and M. Vianello, Compression of multivariate discrete measures and applications, Numer. Funct. Anal. Optim. 36 (2015), 1198–1223.

[23] A. Sommariva and M. Vianello, Polynomial fitting and interpolation on circular sections, Appl. Math. Comput. 258 (2015), 410–424.

[24] A. Sommariva and M. Vianello, Numerical quadrature on the intersection of planar disks, FILOMAT, in press, preprint online at: `http://www.math.unipd.it/~marcov/multidisk.pdf`.